Fabrication of binary volumetric diffractive optical elements in photosensitive chalcogenide AMTIR-1 layers

Alexandre Joerg, Julien Lumeau

HAL Id: hal-01274404
https://hal.science/hal-01274404

Submitted on 26 Mar 2019

Fabrication of binary volumetric diffractive optical elements in photosensitive chalcogenide AMTIR-1 layers

Alexandre Joërg,[1] and Julien Lumeau[1,*]

[1] *Aix Marseille Université, CNRS, Centrale Marseille, Institut Fresnel UMR 7249, 13013 Marseille, France*
Corresponding author: julien.lumeau@fresnel.fr

Abstract: Recording of binary volumetric diffractive optical elements within a 13 µm thick photosensitive chalcogenide layer using an innovative exposure set-up based on digital micro-mirrors devices is demonstrated. Different examples of beam transformations are shown such as the conversion of Gaussian beam into higher order modes or top-hat beam shapers.

Diffractive optical elements are commonly used to convert a Gaussian input beam profile into a target beam profile such as matrices of dots [1], top-hats or vortices [2,3]. These types of elements are used in various applications including: medical lasers [4], 3D imaging [5] or laser material processing [6,7]. They are generally fabricated by local control of the physical thickness of a coated or uncoated glass plate using surface etching techniques associated with a photolithographic process [8]. One of the main drawbacks for these optical components is their sensitivity to dust or scratches. Moreover they require a well-controlled process. In this paper, we propose to produce binary volumetric diffractive optical elements by controlling the local modification of the refractive index of a photosensitive chalcogenide thin film.

To perform this work, $Ge_{33}As_{12}Se_{55}$, a commercial chalcogenide glass known as AMTIR-1, were purchased from Amorphous Material Inc.. This material is well known to provide broad transparency range above 850 nm, high refractive index (n = 2.74 @ 1 µm) and photosensitive properties. Such material was already used in various studies to fabricate thin layers and planar structures using thermal evaporation [9,10] and its photosensitivity was for example used to tune the central wavelength of ring resonators [11] Within this work, we first fabricated 350 nm thick single layers using electron beam physical vapor deposition in a Balzers BAK600 chamber. The residual pressure was ~10^{-6} mbar and the deposition rate was equal to 10 ± 1 A/s. The spectral dependence of the transmission and the reflection of these samples were then measured using a Perkin Elmer Lambda 1050 spectrophotometer and the refractive index, extinction coefficient and physical thickness were determined using Tauc-Lorentz optical dispersion model [12]. This model, derived from Kramers-Kronig relation, was used to account for the strong absorption k>>0.1 in the visible range, this absorption being critical to define the spectral range of photosensitivity. Actually, the transmission and reflection curves reveal three distinct spectral ranges: below 500 nm, AMTIR-1 layers are totally absorbing, above 850 nm, losses are negligible and the layer can be considered as fully transparent, and in between is a transition zone. Using this method, optical band gap energy can also be estimated: Eg = 1.48 eV.
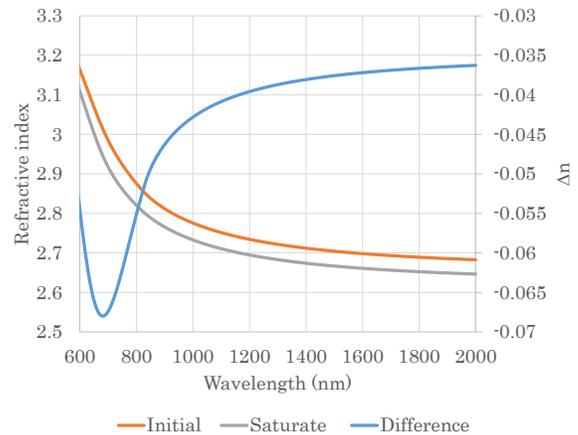

Fig. 1: Refractive index variation at saturation measured in a 350 nm thick AMTIR-1 layer after exposure with a 808 nm laser diode.

The photosensitivity of the layers was then studied using a laser diode centered at 808 nm with a spectral width of 4 nm and a power density of 15 W.cm². This wavelength was chosen to secure large enough absorption to trigger the AMTIR-1 photosensitivity and keep almost uniform exposure throughout the chalcogenide-layer thickness (T_{output} = 50% after propagation within a 13 µm thick layer). As illustrated in Fig. 1, the refractive index is decreasing within increasing the exposure dosage. This variation is spectrally dependent and decreases with wavelength in the region of transparency. A variation of 4.10^{-2} is achieved at 1 µm wavelength with an initial refractive index value of 2.74. Also, optical profilometer measurements have shown that there is no (or negligible) thickness change during this process. In addition, these

data can be easily transferred to thicker layers up to 10+ µm. Finally, it is interesting to note that during exposure, the absorption edge of the AMTIR-1 layer increases up to 1.49 eV, which induces a decrease of the extinction coefficient k at 808 nm from 2.4×10^{-3} down to 1.2×10^{-3}.
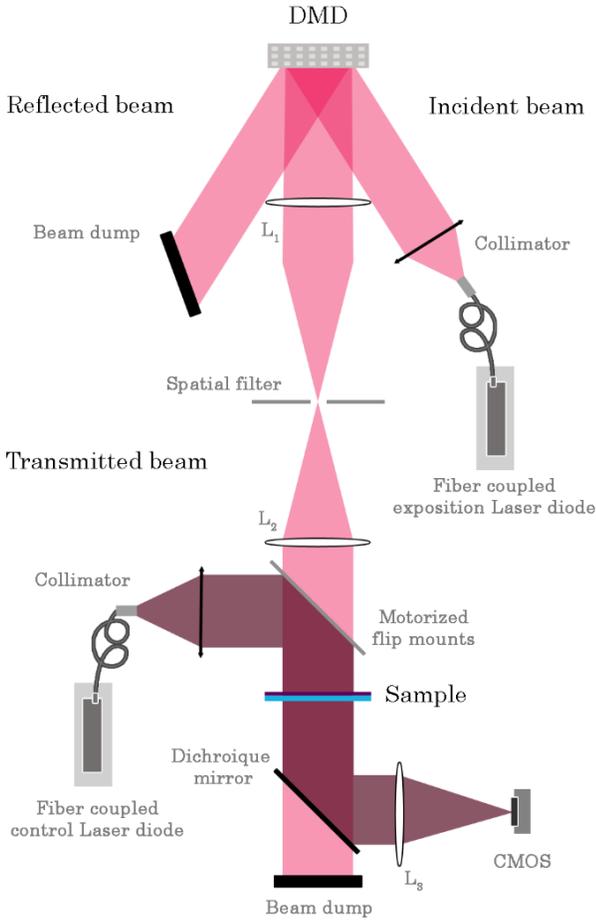

Fig. 2: Experimental setup for the generation of patterned light exposure and in-situ monitoring of the transmission.

We used AMTIR-1 layers in order to fabricate binary volumetric diffractive optical elements (VDOEs) for a 980 nm laser diode. Actually, similar alternative solution using photosensitive PTR glass was proposed some time ago. Volumetric phase elements were recorded within the bulk of 2 mm thick glass plates. However, additional work showed that the use of such thick glass plate present some limitations due to the large interaction length where phase change occur that produce unwanted diffraction pattern in near field which can induce beam distortions in far-field or prevents the recording of elements with small pitch [13]. Thanks to its gigantic photosensitivity, all these limitations of PTR glass phase plates can be prevented. Considering the refractive index variation (∆n) at λ = 1 µm, the total thickness t to deposit on a fused silica substrate to achieve a phase shift between exposed and unexposed regions equal to π is:

$$t = \frac{\lambda}{2\Delta n} \qquad (1)$$

Thus a ~13 µm thick chalcogenide layer was deposited in the same conditions and with the same batch of the 350 nm thick layer. Layer thickness was monitored using a monochromatic optical monitoring system combined with an Inficon quartz monitoring system. This thickness is therefore comparable with the one of standard etched DOEs. However, due to the interferometric behavior of this layer associated with the reflections at the interfaces of the AMTIR-1 layer, inherent high amplitude interferences, which amplitude depends on the incident wavelength and the optical thickness of the layer, appear and will impact the performances of the VDOEs. To avoid this effect, two anti-reflective V-coating for 980 nm were also deposited [14] one (AR1) was designed to minimize reflection at the air/AMTIR-1 interface, the other one (AR2) to minimize the reflection at the AMTIR-1/glass substrate interface. In consequence no interference occur within the AMTIR-1 layer at the centering wavelength, whatever its thickness. The two AR-coating were made using Ta_2O_5 as high index material and SiO_2 as the low one, both material rate deposition was 3 A/s. The designed multilayer structure is therefore:

$$Substrate \ / \ AR2 \ / \ AMTIR-1 \ / \ AR1 \ / \ air \qquad (2)$$

To perform the exposure of the different diffractive patterns on the samples, an exposure set-up was developed (Fig. 2). A 200 µm-fiber-coupled laser diode centered at 808 nm is collimated in a 10 mm diameter beam and is directed toward a DMD Discovery™ 1100 Chip Set including 0.7 XGA Digital Micromirror Device (DMD) produced by Texas Instruments. The DMD is used to modulate the light reflected by a 1024 × 768 micromechanical mirrors matrix with 13.68 µm pitch. Finally, a 4-F system composed with two 100 mm focal length achromatic doublet is used to image, in the focal plane of the second lens, the DMD on the AMTIR-1 layer and avoid diffraction effects. Using this system based on DMDs, it is therefore easy to produce any phase pattern in AMTIR-1 layer as the amplitude profile is directly converted into a phase profile during the exposure. Moreover, the 4-F system having a 1× magnification, the spatial resolution is limited to the 13.68 µm pitch but could be easily decreased by using a magnification below 1. A controlling laser diode combined with a motorized flip mount is also added in the system to monitor in real time the evolution of the VDOE under fabrication and consequently the evolution of the photo-induced refractive index change. This monitoring is performed in far field by measuring the beam profile after diffraction on the VDOE using a CMOS camera situated in the focal plane of a lens. Movies of the evolution of the beam diffracted by the elements during their fabrication can be produced.

To validate our approach, we designed and produced various binary VDOEs. The use of binary VDOEs does not permit to achieve conversion efficiencies as high as

multi-level one, but they have the advantage to provide a simple proof-of concept of this new approach. We first designed Gaussian beam converter. They are mainly used to transform a TM_{00} into a higher order TM_{mn} mode [15,16] and described by Hermits functions.
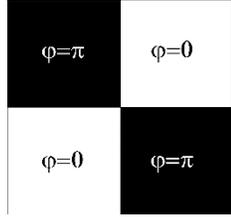

Fig. 3: Four-quadrant Phase mask profile

$$E_{mn} = E_0 H_n\left(\frac{\sqrt{2}x}{\omega_0}\right) Hm\left(\frac{\sqrt{2}y}{\omega_0}\right)\exp\left(\frac{-(x^2 + y^2)}{\omega_0^2}\right) \quad (3)$$

For example transformation of a TM00 mode into a TM11 can be done with a four-quadrant binary profile (Fig. 3). Due to the binary nature of these VDOEs diffraction efficiency is theoretically limited to ~80%.

Other functions were designed such as beam shapers for top-hat beams (square and circular) or beam splitters [17]. These VDOEs were designed using a program based on Gerchberg-Saxton algorithm [18,19]. It uses an iterative Fourier transform to calculate the continuous phase profile, which converts an input beam, generally a Gaussian beam TM00, into the target far field intensity profile. A binarisation was then applied to the final design by taking the absolute value of the $\pm\pi$ continuous profile and then using a threshold of $\pi/2$. Fig. 4 shows the design of some binary VDOEs to convert a TM_{00} Gaussian mode beam into a circular top-hat or a square top-hat beam in far field. Black areas correspond to π phase and white to
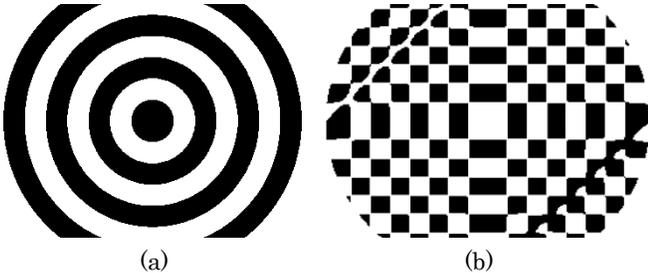

(a)   (b)

Fig. 4: Phase mask profile for (a) circular top hat (b) square top hat. White: Phase = 0, black: Phase = π

null phase. These profiles were applied to the DMD systems and AMTIR-1 layers were exposed with 808 nm diode laser until achieving a π phase shift. Optimal dosage were extracted from preliminary study performed on the 350 nm thick layer and were estimated to be within ~8.102 kJ/cm². High dosage is needed because of the low absorption of AMTIR-1 layers at 808 nm, but could be decreased by using lower exposure wavelength at the expense of a high gradient of induced refractive index throughout the layer thickness.

The evolution of the beam diffracted by these elements during their fabrication is shown in the multimedia file. "Media 1" shows the evolution of the diffracted beam in case of a flat-top beam converter… One can see how the increase of the phase contrast between exposed and unexposed areas allows gradually converting the Gaussian beam into the desired intensity profile. When the intensity profile corresponding to a π-phase shift is achieved, the exposure is stopped. The precise characterization of these VDOEs was carried out ex-situ by placing them in the collimated beam of a single mode fiber-coupled laser source emitting at 980 nm. The Gaussian intensity distribution has a beam diameter at $1/e^2$ of 1.8 mm. The target distribution intensity in far-field was characterized in the focal plane of a 500 mm lens (Fig. 5). The profiles of the beam produced after diffraction on each of the fabricated VDOEs have an excellent correlation with theoretical calculations. To qualify each of them, and to validate the approach, we also calculated the theoretical field distribution in the focal plan of a lens expressed [20] by:

$$U_f(u,v) = \frac{\exp\left(j\frac{k}{2f}(u^2+v^2)\right)}{j\lambda f} TF\left[u_{gauss}.\exp\left(j\varphi_{DOE}(x,y)\right)\right] \quad (4)$$

Where u_{gauss} is the Gaussian field TM00 and φ_{DOE} the VDOE phase pattern. Then theoretical and experimental data were compared in term of loss as follow:

$$L_{tot} = L_{layer} + L_{diff} + L_{mes} \quad (5)$$

L_{layer} is the intrinsic loss of the 13 µm thick chalcogenide film and was measured using a spectrophotometer. It includes loss caused by absorption and scattering and is equal to 9%: L_{diff} is the diffraction loss and is associated with the diffraction efficiency η defined as

$$\eta = \frac{P_d}{P_{tot}} \quad (6)$$

Where P_d and P_{tot} are respectively the signal power in bright region of interest. Finally, L_{mes} is the loss associated with the measurement errors and sensitivity and cannot experimentally be differentiated from L_{diff}. Compared to theoretical efficiency, a diffraction loss of ~3% was measured on each component. This difference can be associated with a phase difference that did not quite reached π in the exposed area. For example, an error of 5% on the phase shift can explain a 2% diffraction loss efficiency. Other possible reason of this decrease are associated with measurements errors, for example an M² larger than 1 for the characterization Gaussian beam at 980 nm or instabilities of the of the laser diode that are within 0.05 dB.

In addition an error function (EF) [21] was defined to quantify the deviation between the theoretical and experimental diffraction patterns

$$EF = \sqrt{\frac{1}{m \times n - 1} \sum_m \sum_n \left(I_{mes}(m,n) - I_{th}(m,n)\right)^2} \qquad (7)$$

EF's values are gathered in Table 1, their low values validate the good correlation between theoretical and experimental beam profiles in the focal plane of the lens (Fig. 6)
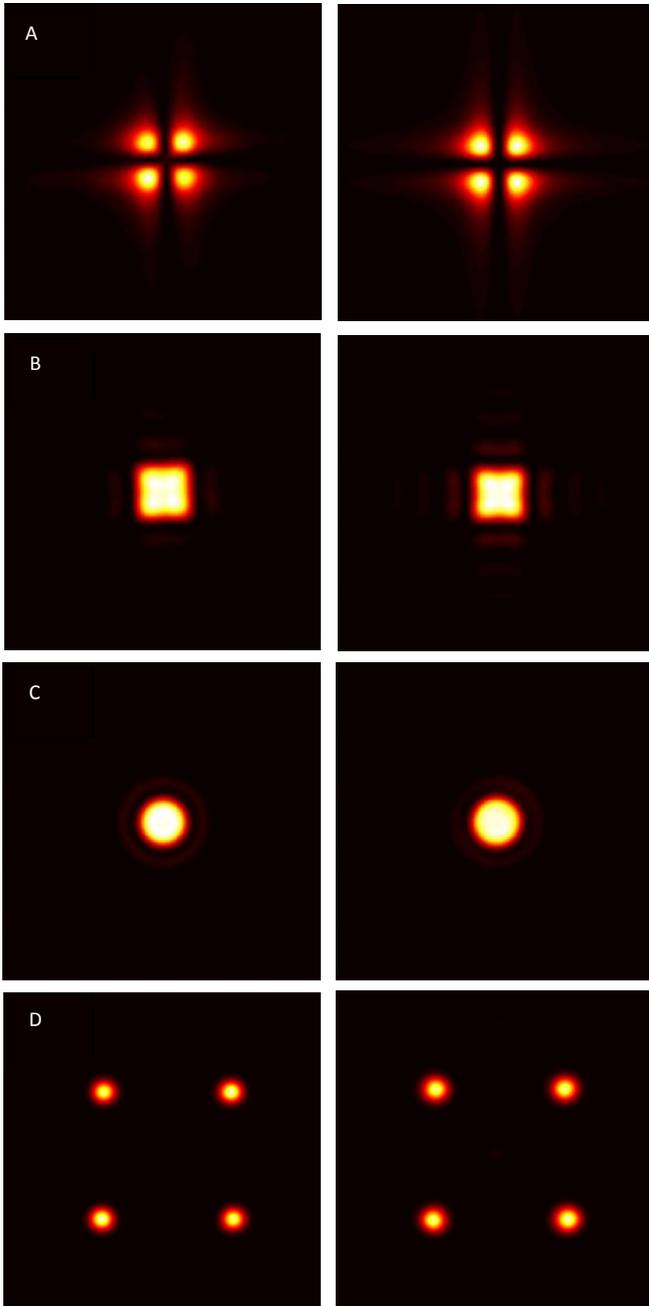
A

B

C

D

Fig. 6: Far-field diffraction patterns of a Gaussian beam after propagation through a phase mask at the focal plane of a 500 mm lens. Left side experimental results. Right side theoretical results. A: four quadrant, B: square top hat, C: circular top-hat and D: dot-matrix – "Media 1"

Table 1. Criteria for diffraction pattern accuracy

Function name	EF1
Gaussian Converter	2%
Circular Top-hat	1,1%
Square Top-hat	1,4%
Dot Matrix	1,8%

The method of producing volumetric diffractive optical elements recorded within thin film chalcogenide layers by a local control of the refractive index was demonstrated. A
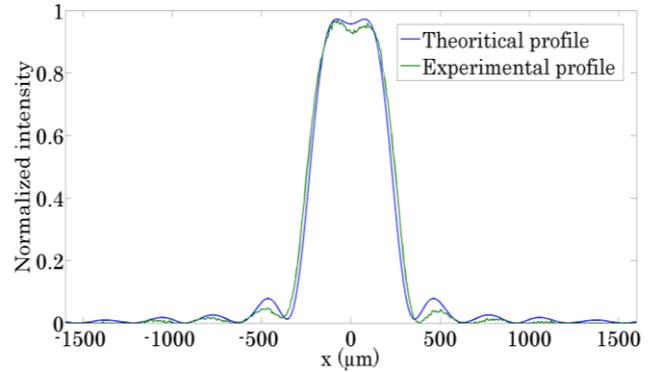
Fig. 5: Theoretical and experimental Intensity profile of the square top-hat beam in horizontal direction

versatile exposure set-up using a DMD that allows easily producing different diffractive patterns was described. Different prototype such as a Gaussian beam converter, circular or square top-hat, and beam splitter were produced with near theoretical profiles.

References
1. G. Wernicke, Opt. Lett. **32**, 448 (2007).
2. A. Sabatyan, B. Meshginqalam, Appl. Optics. **53**, 5995 (2014).
3. M. Duocastella, C.B. Arnold, Laser Phot. Rev. **6**, 607 (2012).
4. M. Golub, I. Grossinger, Contact Lens Asso. of Ophthalmologists J. **22**, 245 (1996).
5. M. Bauer, D. Griessbach, A. Hermerschmidt, S. Krüger, M. Scheele, A. Schichmanow, Optics Expresss. **16**, 20241 (2008).
6. S. Haas, G. Schöpe, C. Zahren, H. Stiebig, Appl. Phy. A. **92**, 755 (2008).
7. J. Cordingley, Appl. Opt. **23**, 2538 (1993).
8. T. Fujita, H. Nishihara, J. Koyama, Opt. Lett. **6**, 613 (1981).
9. R. A. Jarvis, R. P. Wang, A. V. Rode, C. Zha, B. Luther-Davies, J. of Non-Crystalline Solids. **353**, 947 (2007).
10. R. P. Wang, A. V. Rode, S. J. Madden, C. J. Zha, R. A. Jarvis, B. Luther Davies, J. of Non-Crystalline Solids. **353**, 950 (2007).
11. N. Singh, D. D. Hudson, R. Wang, E. C. Mägi, D-Y. Choi, C. Grillet, B. Luther-Davies, S. Madden, B .J. Eggleton, Opt. Express. **23**, 8681 (2015).
12. L. Gao, F. Lemarchand, M. Lequime, Thin Solid Films.. **520**, 501 (2011).
13. M.A. Segall, PhD thesis, University of Central Florida, (2013)
14. F. Lemarquis, Appl. Opti. **53**. 229 (2014).
15. M. Segall, V. Rotar, J. Lumeau, S. Mokhov, B. Zeldovich, L. B. Glebov, Opt. Lett. **37**, 1190 (2012).
16. F. J. Salgado-Remacha, Appl. Opt. **53**, 6782 (2014).
17. J. J Yang, M. R. Wang, Opti. Engin. **42**, 3106 (2003).

18. R. G. a. W. Saxton, Optik. **35**, 237 (1972).
19. M. T. Eismann, A. M. Tai, J. N. Cederquist, Appl. Opt. **28**, 2641 (1989)
20. J. W. Goodman, Paris: Masson&Cie, (1972).
21. H. Duadi, Z. Zalevsky, Opt. Com. **283**,. 951 (2010)

Full references

1. G. Wernicke, «Binary diffractive beam splitters with arbitrary diffraction angles,» Optics Letters. vol. 32, n° 15, pp. 448-450, (2007).
2. A. Sabatyan, B. Meshginqalam, «Generation of annular beam by a novel class of Fresnel zone plate,» Applied Optics. vol. 53, n° 126, pp 5995-6000 (2014).
3. M. Duocastella, C.B. Arnold, «Bessel and annular beams for materials processing,» Laser Photonics Rev. vol. 6, n° 5,pp. 607-621, (2012).
4. M. Golub, I. Grossinger, «Diffractive optical elements for biomedical applications,» Contact Lens Association of Ophthalmologists Journal. vol. 22, n°14, pp. 245-249, (1996).
5. M. Bauer, D. Griessbach, A. Hermerschmidt, S. Krüger, M. Scheele, A. Schichmanow, «Geometrical camera calibration with diffractive optical elements,» Optics Expresss. vol. 16, n°25, pp. 20241-20248, (2008).
6. S. Haas, G. Schöpe, C. Zahren, H. Stiebig, «Analysis of the laser ablation processes for thin-film silicon solar cells,» Applied Physics A. vol. 92, pp. 755-759, (2008).
7. J. Cordingley, «Application of a binary diffractive optic for beam shaping in semiconductor processing by lasers,» Applied Optics, vol. 23, n° 114, pp. 2538-2542, (1993).
8. T. Fujita, H. Nishihara, J. Koyama, «Fabrication of micro lenses using electon-beam lithography,» Optics Letters. vol. 6, n°112, pp 613-615, (1981).
9. R. A. Jarvis, R. P. Wang, A. V. Rode, C. Zha, B. Luther-Davies, «Thin film deposition of Ge33As12Se55 by pulsed laser deposition and thermal evaporation: Comparison of properties,» Journal of Non-Crystalline Solids. vol. 353, pp. 947-949, (2007).
10. R. P. Wang, A. V. Rode, S. J. Madden, C. J. Zha, R. A. Jarvis, B. Luther Davies, «Structural relaxation and optical properties in amorphous Ge33As12Se55 films,» Journal of Non-Crystalline Solids. vol. 353, pp. 950-952, (2007).
11. N. Singh, D. D. Hudson, R. Wang, E. C. Mägi, D-Y. Choi, C. Grillet, B. Luther-Davies, S. Madden, B .J. Eggleton, «Positive and negative phototunability of chalcogenide (AMTIR-1) microdisk resonator,» Optics Express. vol. 23, n° 17, pp. 8681-8686, (2015).
12. L. Gao, F. Lemarchand, M. Lequime, «Comparison of different dispersion models for single layer optical thin film index determination,» Thin Solid Films. vol. 520, pp. 501-509, (2011).
13. M. A. Segall, , «Volume Phase masks in photo-thermo-refractive glass,» Optics & Photonics, M.S. University of Central Florida, p. 154, (2013)
14. F. Lemarquis, «Athermal compensation of the stress-induced surface deflection of optical coatings using iso-admittance layers,» Applied Optics. vol. 53, n° 14, pp. 229-236, (2014).